Electronic Supplementary Material (ESI) for Physical Chemistry Chemical Physics.

Supporting Information: Cs^+ conductance in graphene membranes with Ångström-scale pores: the role of pore entrance geometry.

Enrique Wagemann,[†] Na Young Kim,[‡,¶,§] and Sushanta K. Mitra[*,§]

†*Departamento de Ingeniería Mecánica, Facultad de Ingeniería, Universidad de Concepción, Concepción, Chile, 4070409*

‡*Institute for Quantum Computing, University of Waterloo, 200 University Ave. West, Waterloo, Ontario, Canada, N2L 3G1*

¶*Department of Electrical and Computer Engineering, University of Waterloo, 200 University Ave. West, Waterloo, Ontario, Canada, N2L 3G1*

§*Micro & Nano-Scale Transport Laboratory, Waterloo Institute for Nanotechnology, Department of Mechanical and Mechatronics Engineering, University of Waterloo, Waterloo, Ontario N2L 3G1*

E-mail: skmitra@uwaterloo.ca

Contents

1 Membrane construction

The simulated membranes are built by stacking 14 graphene sheets, and then removing the central one. Different pore entrance geometries are constructed by removing rows of carbon atoms from the leftmost edges of the internal graphene sheets (see figure fig. S1 a). Each row is defined from the basic unit cell employed to construct each sheet (figures fig. S1 b and c). Before having a row removed, each graphene layer contains 31 rows. After the row removal, a hydrogen atom is included to saturate each edge carbon atom.

Table S1: Number of removed rows of carbon atoms for all of the simulated systems.

System	L3	L2	L1	U1	U2	U3
Sharp	0	0	0	0	0	0
AA1	1	2	3	0	0	0
AA2	2	4	6	0	0	0
AA3	3	6	9	0	0	0
AS1	1	2	3	3	2	1
AS2	2	4	6	6	4	2

System	L3	L2	L1	U1	U2	U3
AS3	3	6	9	9	6	3
ASC1	0	0	16	0	0	0
ASC2	0	16	16	0	0	0
SSC1	0	0	16	16	0	0
SSC2	0	16	16	16	16	0

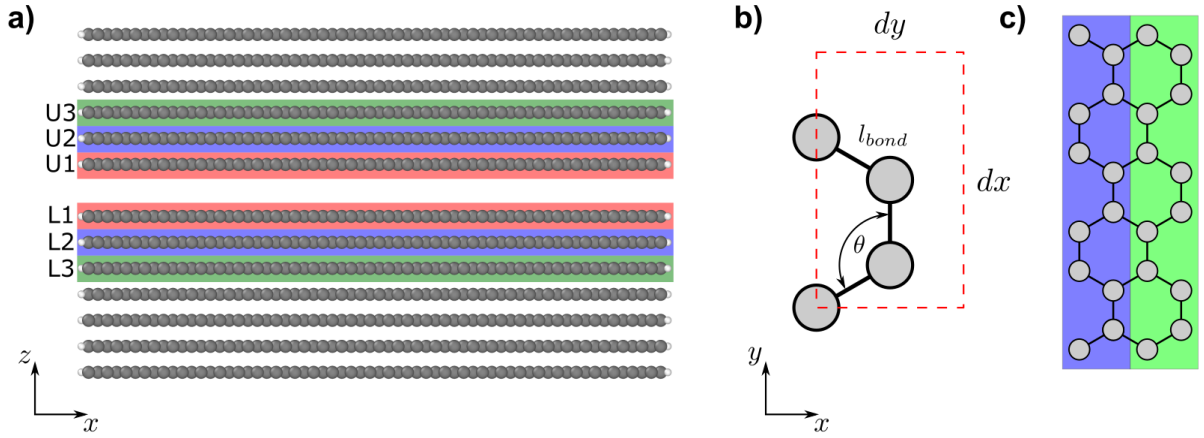

Figure S1: Row removal to modify the membrane entrance geometry. a) Rows of carbon atoms are removed from internal sheets L1, L2, L3, U1, U2, and U3. b) Basic unit cell employed to build each graphene layer. c) schematic representation of a removed row. Blue and green background colors depict two different rows

2 Simulation snapshots

A snapshot for all the simulated cases is presented in figures figs. S2, S3, S4, S5, S6. In these figures, red circles depict oxygen atoms; white circles depict hydrogen atoms; gray circles depict carbon atoms; green circles depict Cs^+ ions; and purple circles represent Cl^- ions. The external black lines represent the boundaries of the simulation box.

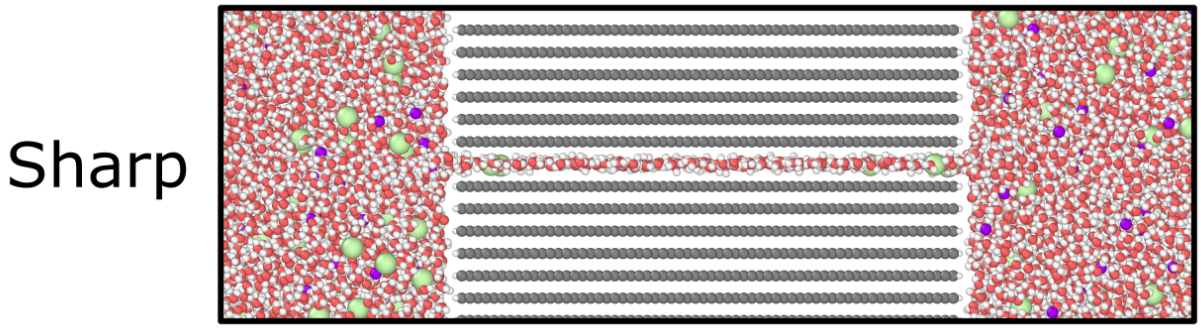

Figure S2: Sharp system

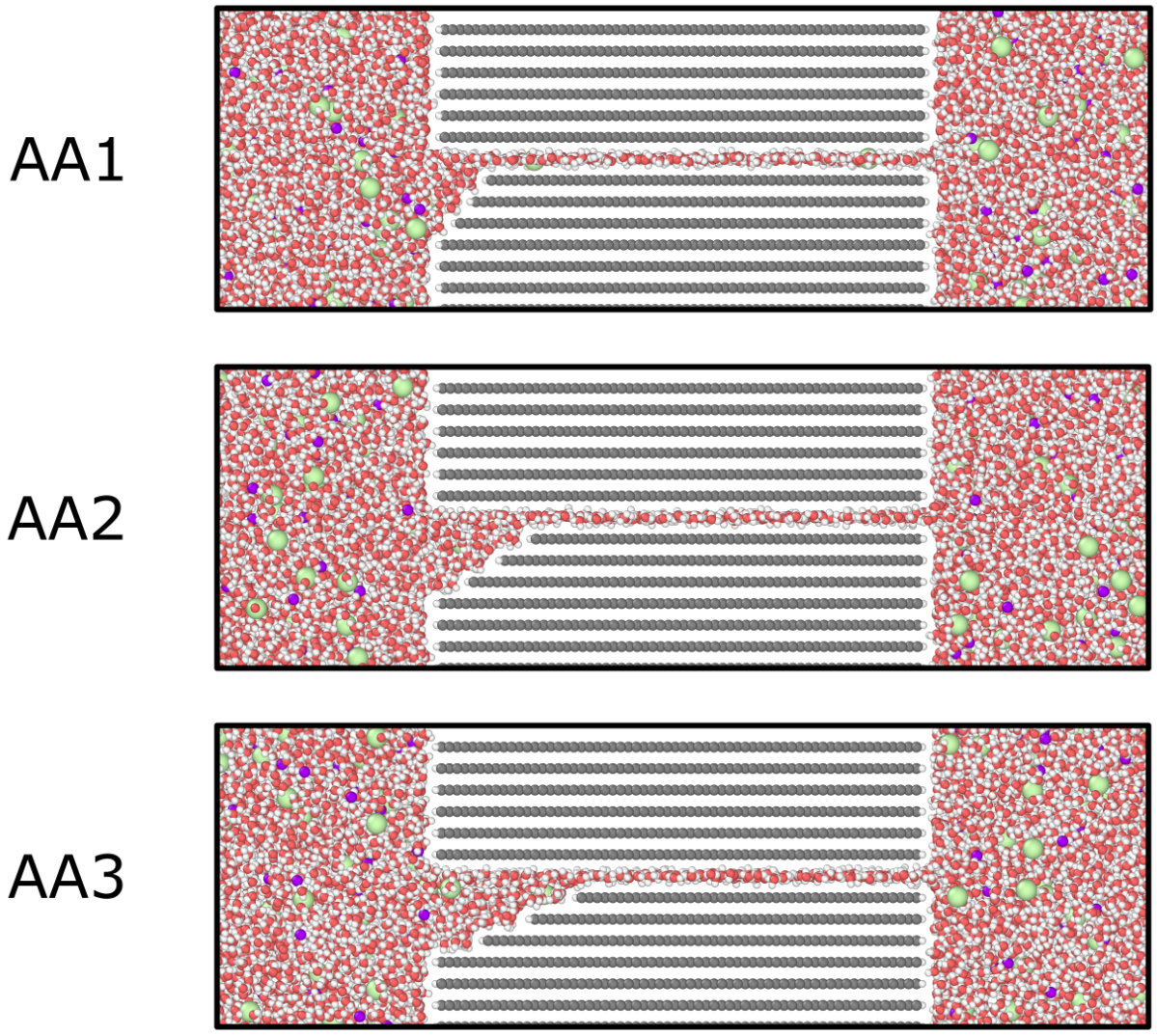

Figure S3: Asymmetric Angular (AA) systems

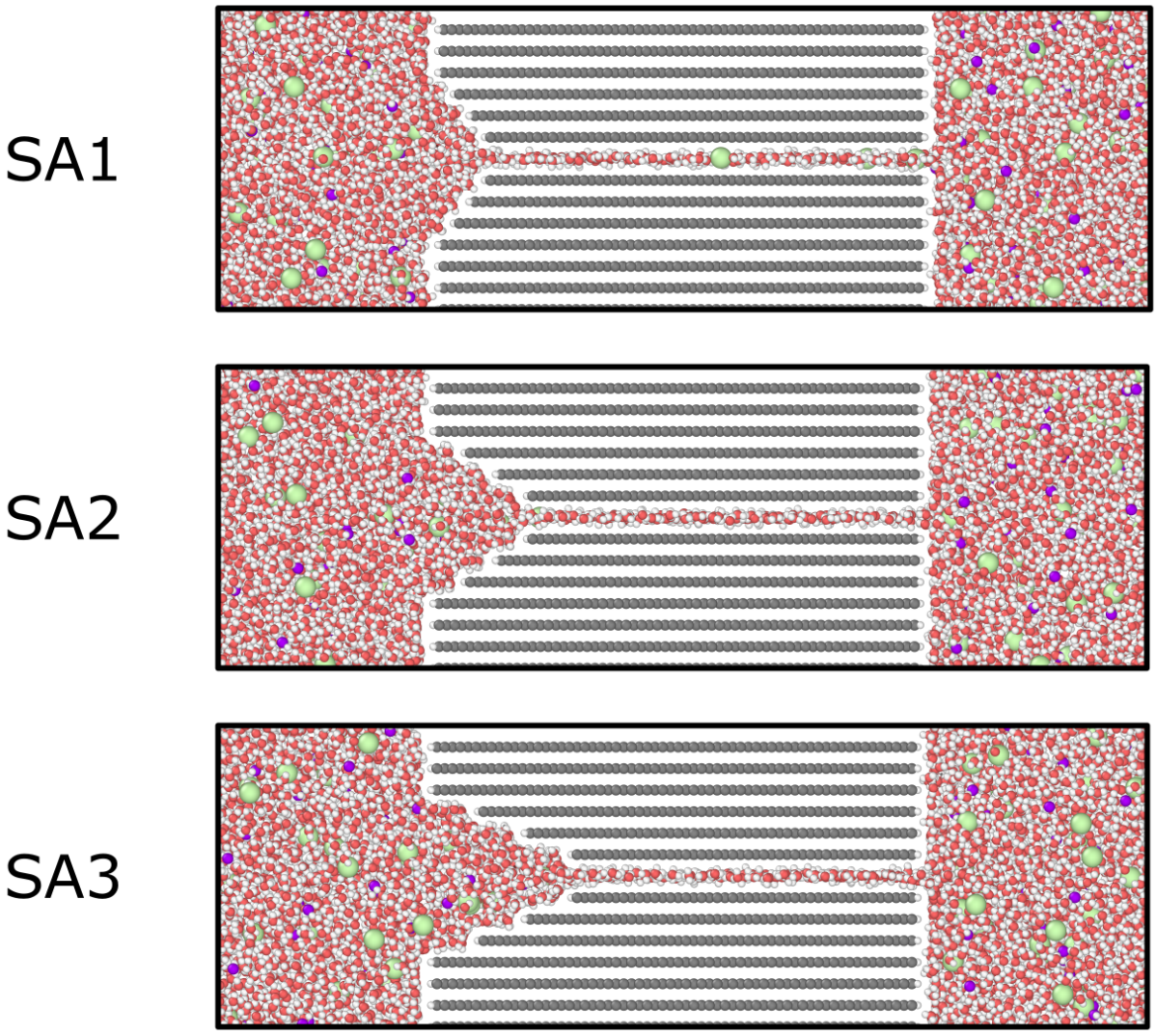

Figure S4: Symmetric Angular (SA) systems

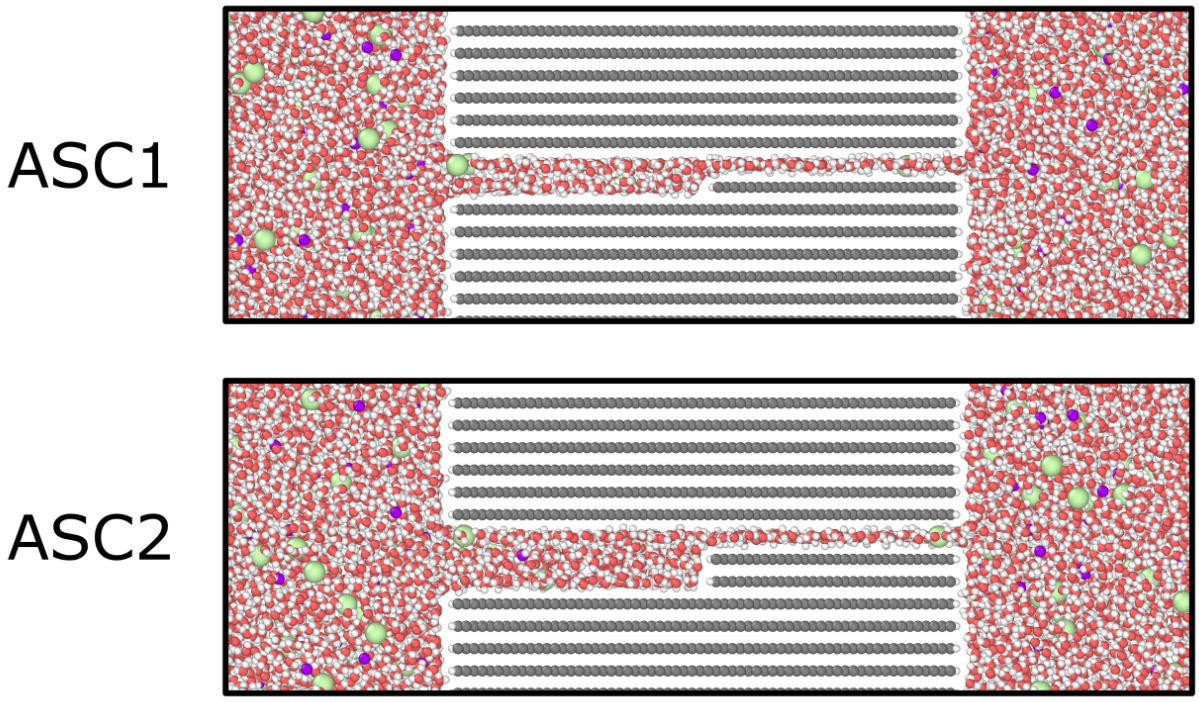

Figure S5: Asymmetric Sudden Contraction (ASC) systems

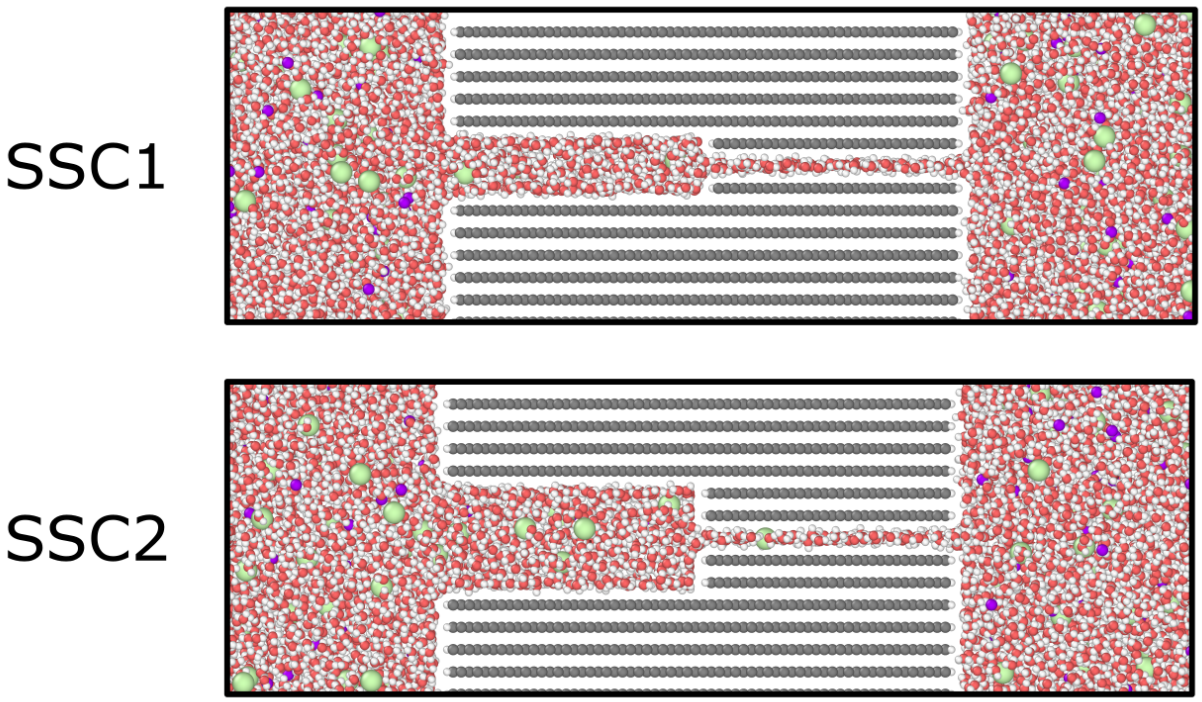

Figure S6: Symmetric Sudden Contraction (SSC) systems

3 Number of water molecules required to fill the systems

In order to maintain similar CsCl concentrations in the reservoirs across all of the studied cases, additional water molecules are added to each system. The required number of water molecules is estimated from the number of water molecules required to fill each channel with pure water. We estimate this number, for each of the simulated cases, by conducting simulations in the NPT ensemble at a temperature of 300 K and 1 bar. Each of the simulated systems consists of two reservoirs filled with pure water and the graphene (GE) membrane separating them (see figure fig. S7). All these systems contain 3156 water molecules and the characteristics of the GE membrane are identical to the ones of the simulations discussed in the main article. The barostatting is applied only in the $x-$direction. The simulations are conducted as follows: first, the system is equilibrated during 250 ps in the NVT ensemble at a temperature of 300,K. Then, 4 ns are simulated in the NPT ensemble. During the last 2 ns, the average no. of water molecules inside of the channel is computed. The van der Waals size of carbon atoms (a diameter of ca. 3.4 Å) is considered to determine the limits of the channel in the $x-$direction. The computed average number of water molecules inside the channel ($N_{w,\text{channel}}$) for each of the studied membrane geometries are presented in Table S2, along with the total number of water molecules employed in the simulations discussed in the main article ($N_{w,\text{total}}$).

Table S2: Number of water molecules N_w considered for each system.

System	$N_{w,\text{channel}}$	$N_{w,\text{total}}$
Sharp	298	3850
AA1	325	3877
AA2	377	3929
AA3	430	3982
AS1	356	3908
AS2	459	4011

System	$N_{w,\text{channel}}$	$N_{w,\text{total}}$
AS3	560	4112
ASC1	426	3978
ASC2	572	4124
SSC1	570	4122
SSC2	843	4395

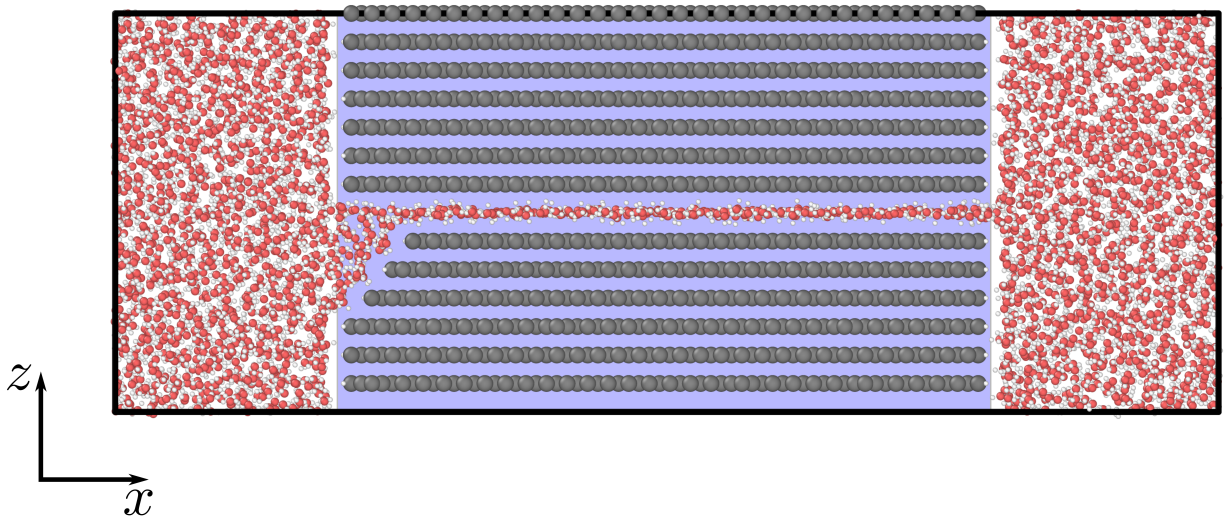

Figure S7: Employed system to determine the number of water molecules required to fill each channel. The blue blox represents the limits considered to compute the number of water molecules inside the channel. The presented snapshot corresponds to the AA1 system.

4 Non-bonded interaction parameters

In this study, all the vdW interactions are modeled using a 12-6 Lennard-Jones (LJ) potentinal. Table S3 summarizes the employed parameters for the non-bonded interactions in our simulations. The LJ parameters for the interactions between atoms of different types are obtained by employing Lorentz-Berthelot combining rules ($\sigma_{ij} = (\sigma_i + \sigma_j)/2$; $\varepsilon_{ij} = \sqrt{\varepsilon_i \varepsilon_j}$).

Table S3: Non-bonded interaction parameters

Atom type	σ_i (Å)	ε_i(kcal/mol)	$q_i(e)$
O^{S1}	3.1589	0.1852	0.0
H^{S1}	0.0	0.0	0.5564
M^{S1}	0.0	0.0	−1.1128
C^{S2}	3.39967	0.086	0
$C_{CH}{}^{S2}$	2.985	0.046	−0.115
$H_{CH}{}^{S2}$	2.42	0.0301	0.115
$Cl^{-\,S3,S4}$	4.92	0.0116615	−1
$Cs^{+\,S3,S4}$	3.36	0.3944318	1
$Na^{+\,S3,S4}$	2.18	0.1684375	1

5 Length of the simulation box in the x-direction

The employed length of the simulation box for each simulated cases is presented in Table S4. The reported length is obtained after 4 ns of equilibration in the NPT ensemble. Notice that, in all cases, the simulation box has lengths of 3.4 nm and 4.8 nm in $y-$ and $z-$directions, respectively.

Table S4: Length of the simulation box in the $x-$direction for each simulated case.

System	L_x (Å)	System	L_x (Å)
Sharp	148.36	AS3	146.77
AA1	147.43	ASC1	147.23
AA2	147.13	ASC2	147.34
AA3	147.13	SSC1	147.56
AS1	147.29	SSC2	147.08
AS2	146.59		

6 Ionic current - Voltage (I-V) curves

The Ionic current - Voltage ($I-V$) curves are presented for the Sharp, AA, SA, ASC, and SSC membrane geometries are presented in figs. S8, S9, S10, S11, and S12, respectively. In all of the presented plots, error bars are estimated from the standard error of the computed ionic current.

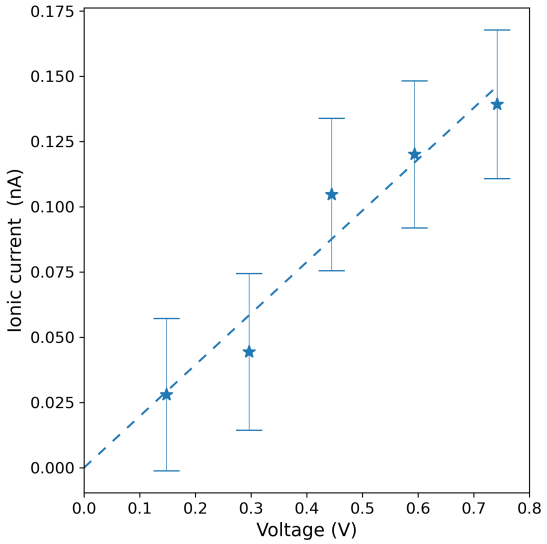

Figure S8: Ionic current - voltage ($I-V$) curves for the Sharp case.

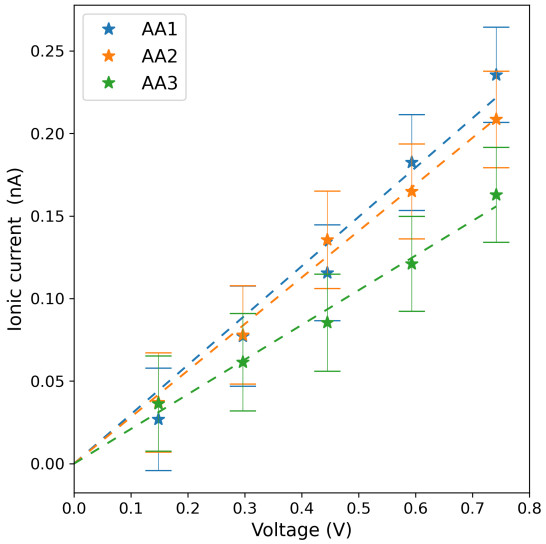

Figure S9: Ionic current - voltage ($I-V$) curves for the AA cases.

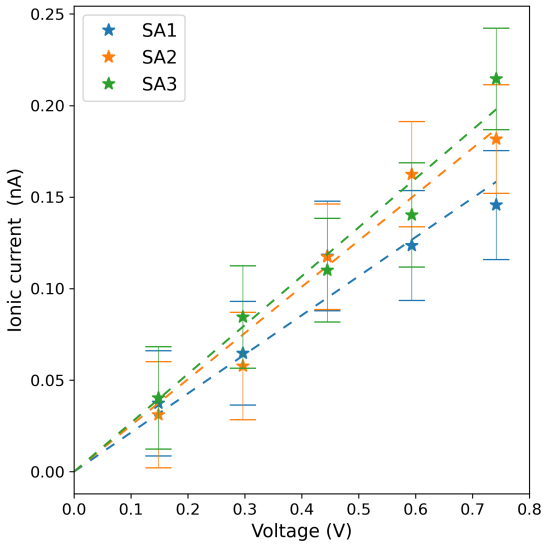

Figure S10: Ionic current - voltage ($I-V$) curves for the SA cases.

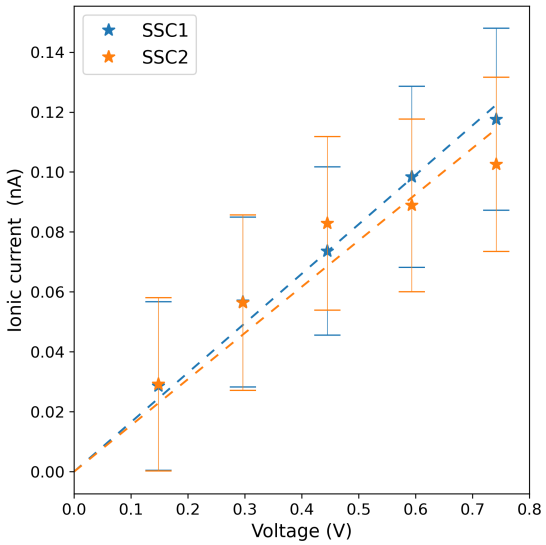

Figure S11: Ionic current - voltage ($I-V$) curves for the ASC cases.

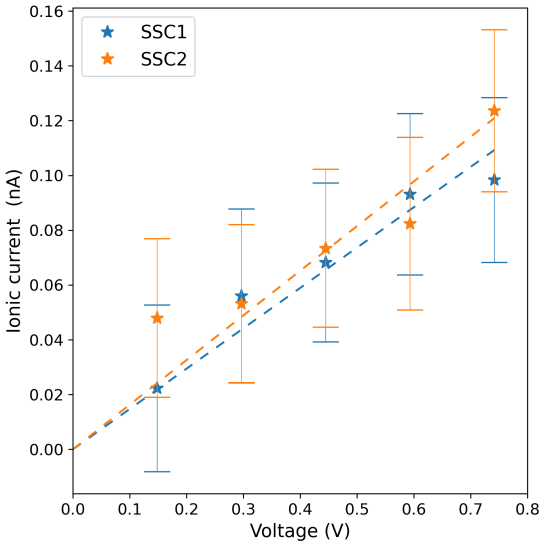

Figure S12: Ionic current - voltage ($I-V$) curves for the SSC cases.

7 Potential of mean force: ASC and SSC cases

The estimated potential of mean force (PMF) for the ASC and SSC cases are presented in Figs. S13 and S14, respectively.

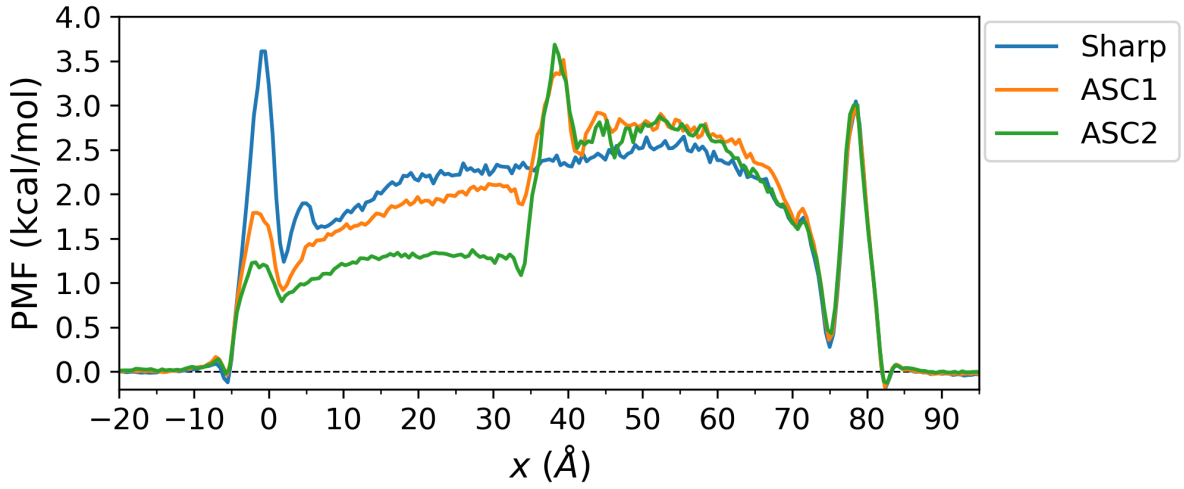

Figure S13: Potential of Mean Force (PMF) for the ASC cases.

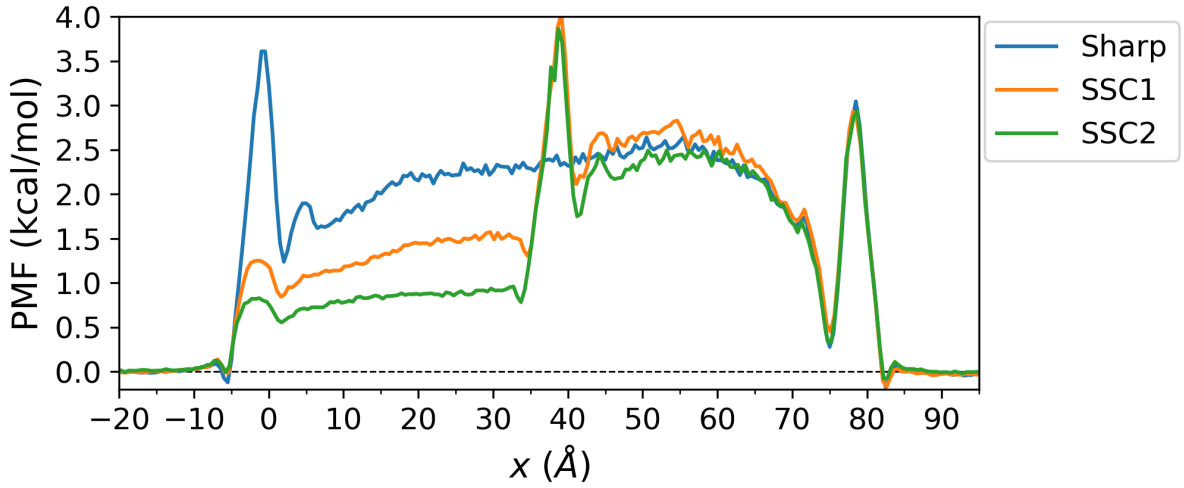

Figure S14: Potential of Mean Force (PMF) for the SSC cases.

8 Hydration shell structure

The structure of the hydration shell is characterized by the number of oxygen atoms at its first and second layers, i.e., the coordination number (CN) of each layer. The CN at each layer is determined locally by employing a binning sampling method. In each bin, the number of oxygen atoms in each layer surrounding each Cs^+ ion is determined by integrating the radial density function (RDF). For the first hydration layer, the RDF is integrated up to its first minimum. In contrast, the number of Oxygen atoms in the 2nd hydration layer is determined by integrating the RDF between its first and second minimums. The RDF is computed inside the membrane by considering a region of 4 nm at its center. The RDF for the Cs^+-O and $Cs^+ - H$ at this zone is presented in figure fig. S15. For bulk solution, the RDF is computed at the outer parts of the simulation box by considering a region of 1 nm in $x-$direction. The RDFs for bulk solution is presented in figure fig. S16.

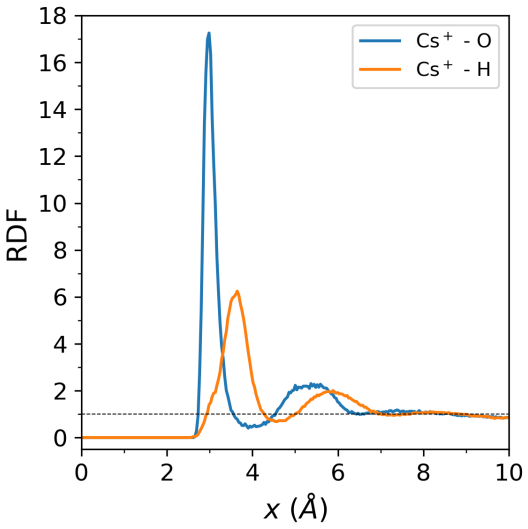

Figure S15: Radial density function for the Cs^+-O and Cs^+-H pairs for an ion confined in the $h_{eff} = 3.4$ Å channel

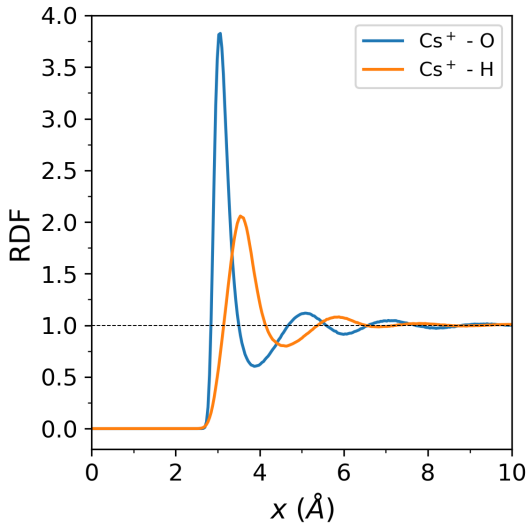

Figure S16: Radial density function for the Cs^+-O and Cs^+-H pairs for an ion in bulk aqueous solution

In bulk solution, i.e., outside the membrane, an average CN of 7.9 ± 0.3 was computed for the first hydration layer. Such a value is in close agreement with the values reported by Döpke et al.[S4]. The number of oxygen atoms in the second hydration layer for a Cs^+ in bulk

solution was determined to be 20.4 ± 1.2. When entering the thinner part of each membrane (with $h_{eff} = 3.4$ Å), the number of oxygen atoms in the first hydration layer is reduced to an average of 5.0 ± 0.1 atoms, while it is reduced to 9.3 ± 0.3 atoms in the second hydration layer. Such a reduction is a result of the dimensionality associated with the 2D confinement of ions in the sub-nm part of the membrane. It is to be noted that while the CN is reduced when entering the membrane, the distance between Cs^+ and Oxygen atoms is reduced from ca. 3.05 Å in bulk solution to 2.95 Å in 2D confinement. The reduced distance ensures a stronger interaction between ion and water molecules, which allows compensating for some of the shed water molecules

9 2D probability function and x-compontent of the electric field-resultant force.

In this section, we present the 2D PDF and distribution of the $x-$component of the force exterted by electric field generated by the CH functional group for the cases not shown in the main article.

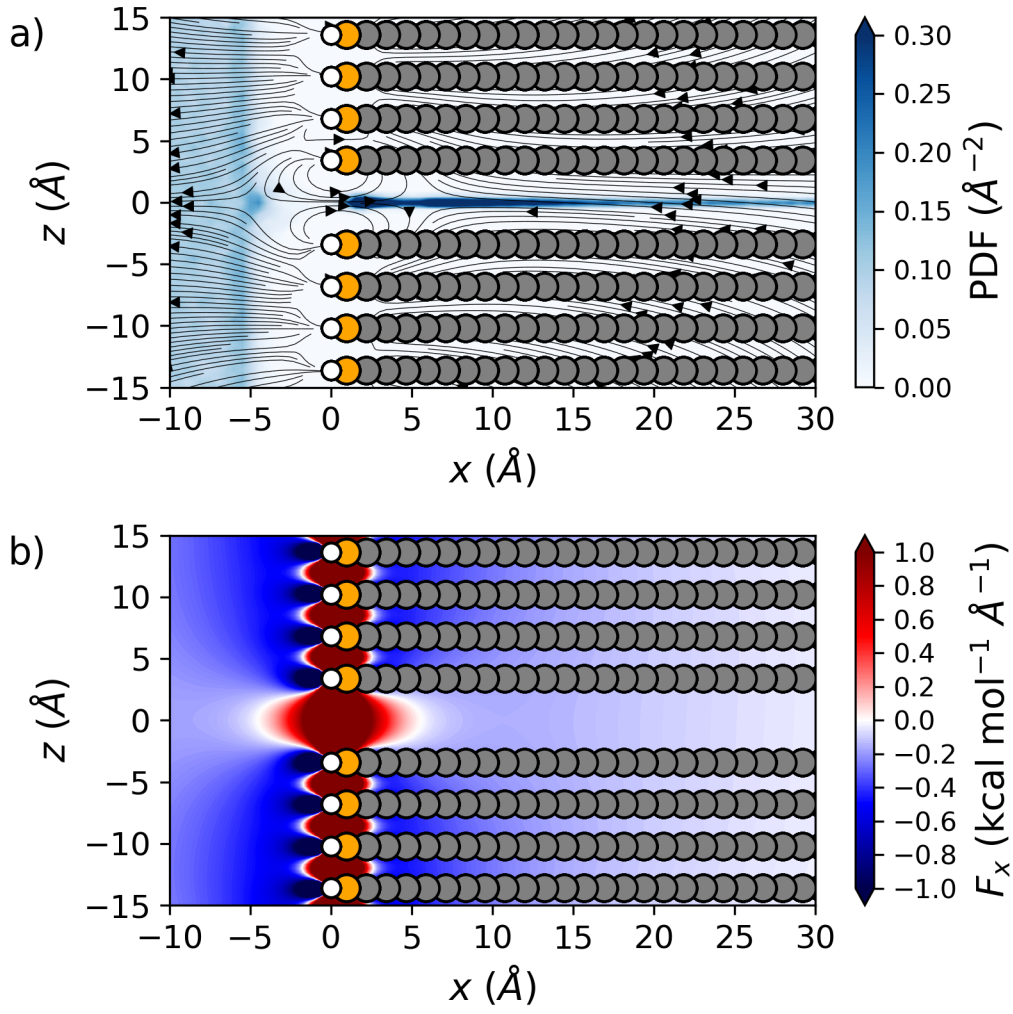

Figure S17: Probability Density and Electric Field Analysis for the Sharp case. a) 2D Probability Density Function (PDFs). b) x-direction component of the net force (F_x) exerted by the functional group-generated electric field.

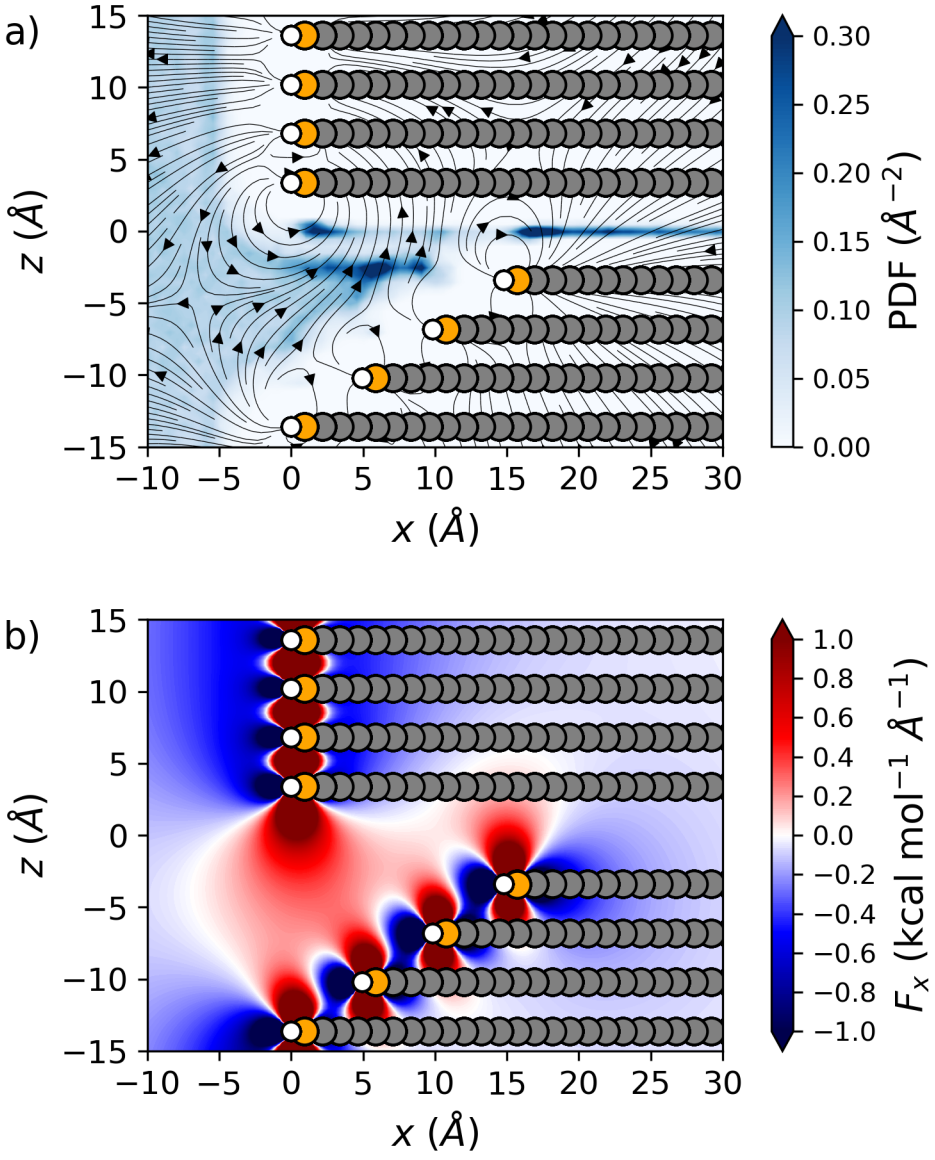

Figure S18: Probability Density and Electric Field Analysis for the AA2 case. a) 2D Probability Density Function (PDFs). b) x-direction component of the net force (F_x) exerted by the functional group-generated electric field.

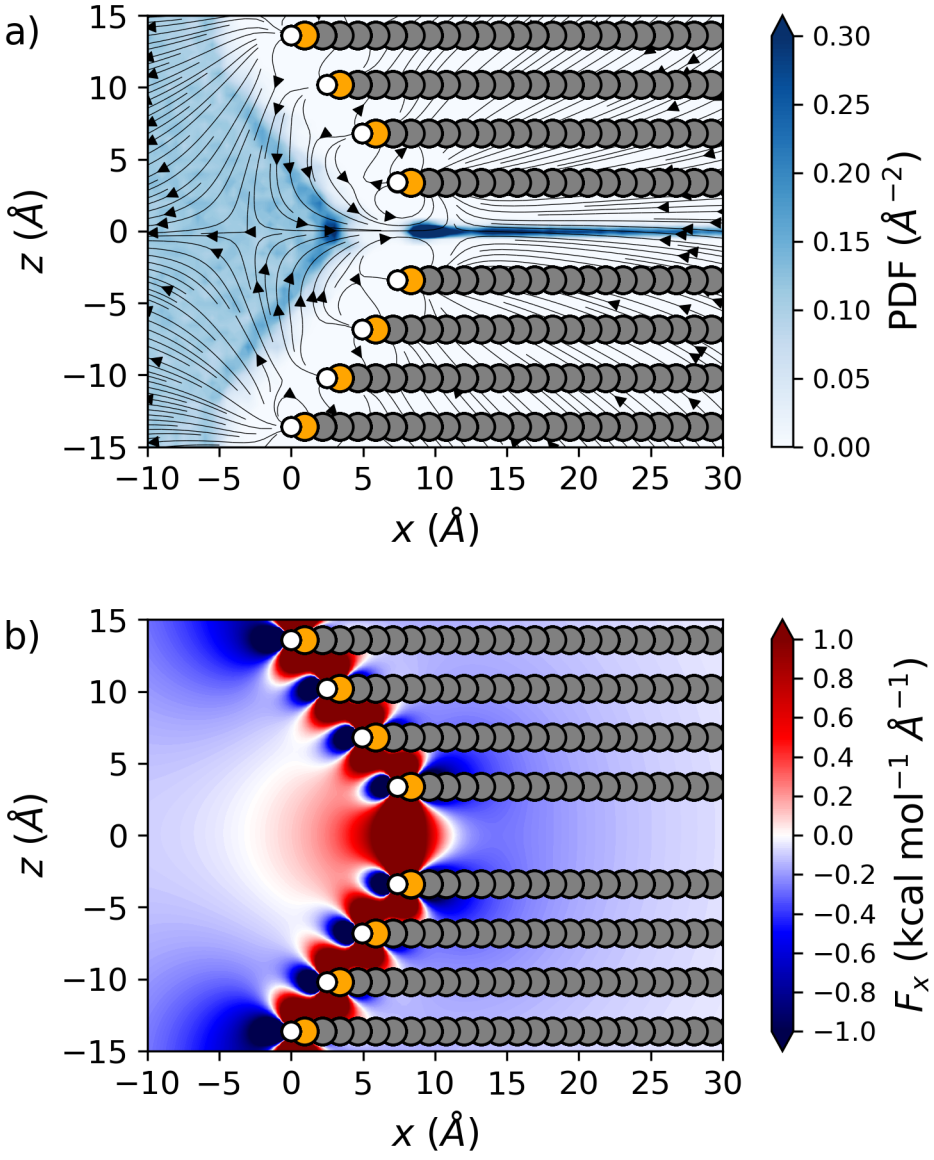

Figure S19: Probability Density and Electric Field Analysis for the SA1 case. a) 2D Probability Density Function (PDFs). b) x-direction component of the net force (F_x) exerted by the functional group-generated electric field.

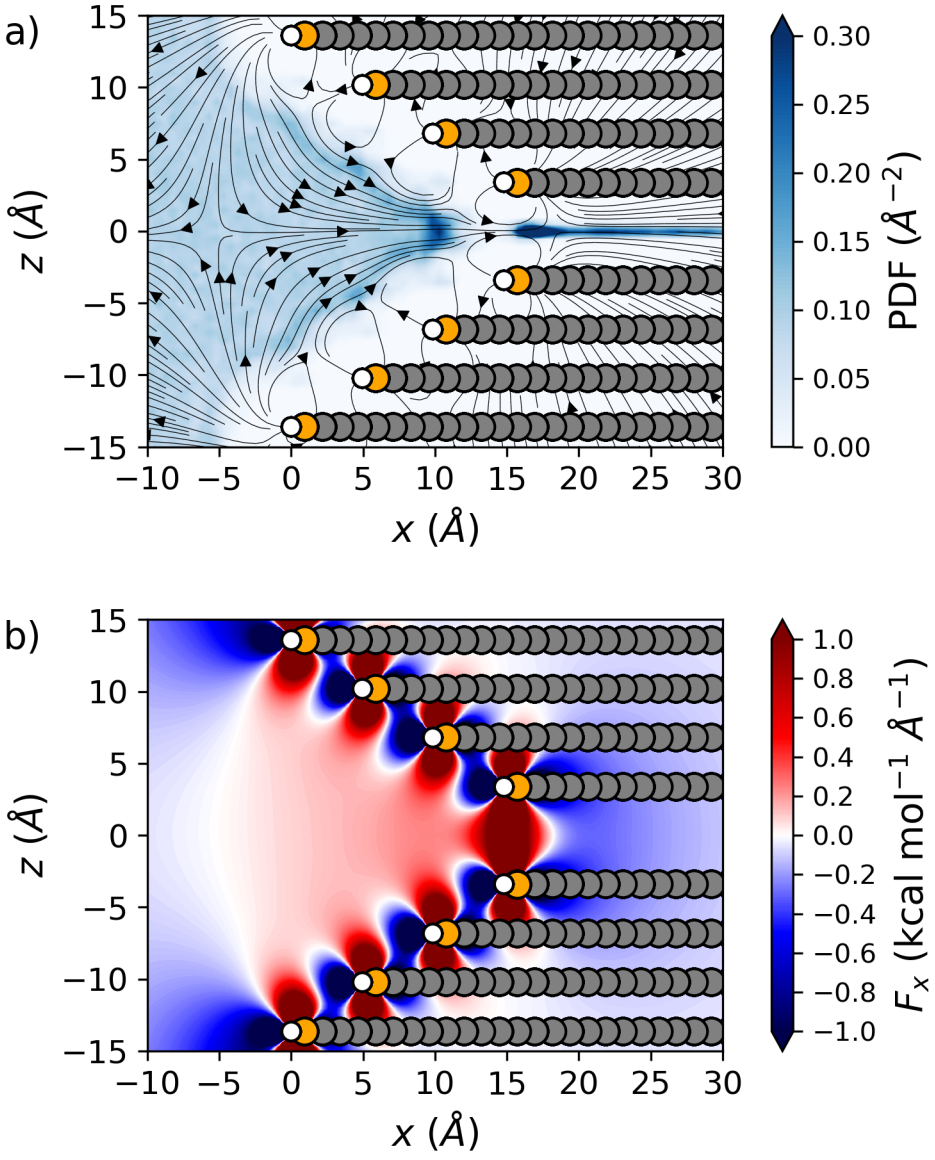

Figure S20: Probability Density and Electric Field Analysis for the SA2 case. a) 2D Probability Density Function (PDFs). b) x-direction component of the net force (F_x) exerted by the functional group-generated electric field.

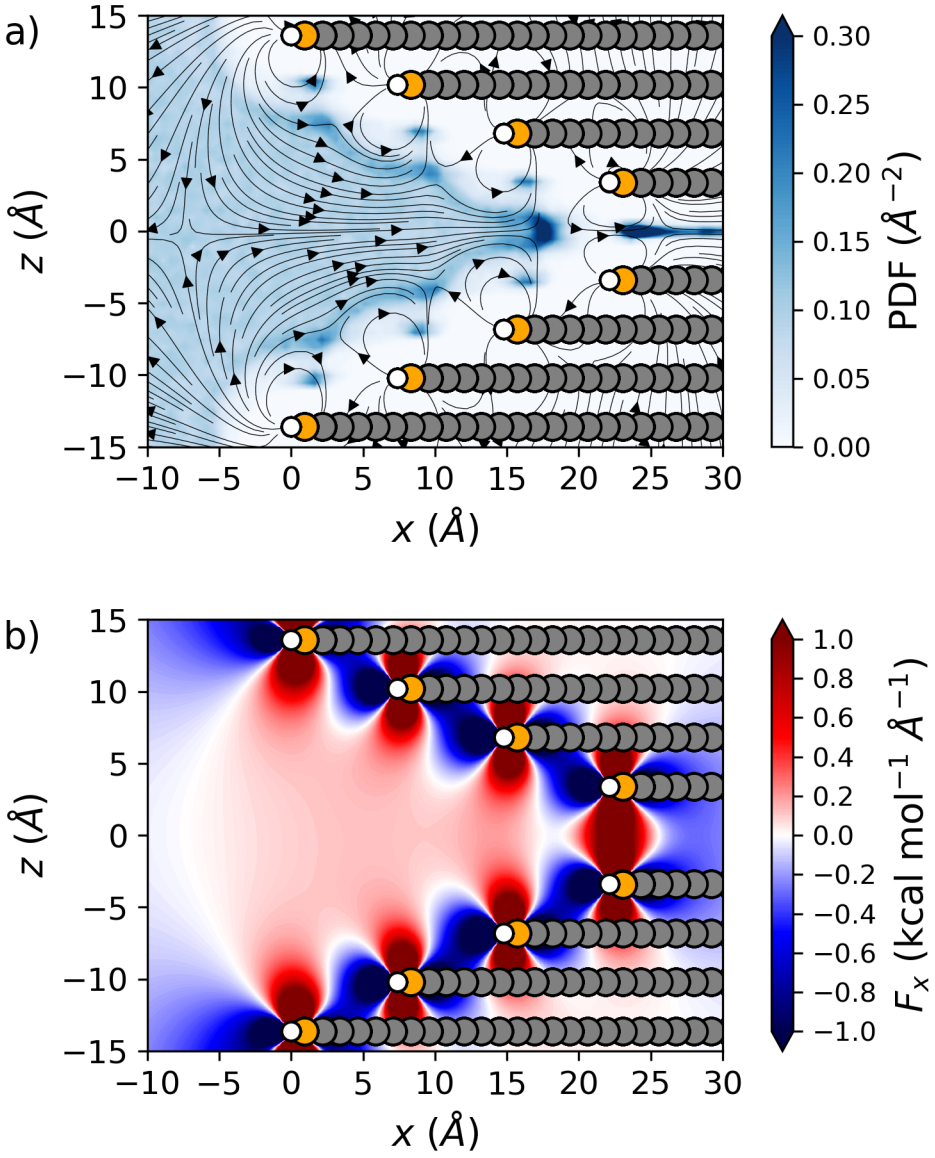

Figure S21: Probability Density and Electric Field Analysis for the SA3 case. a) 2D Probability Density Function (PDFs). b) x-direction component of the net force (F_x) exerted by the functional group-generated electric field.

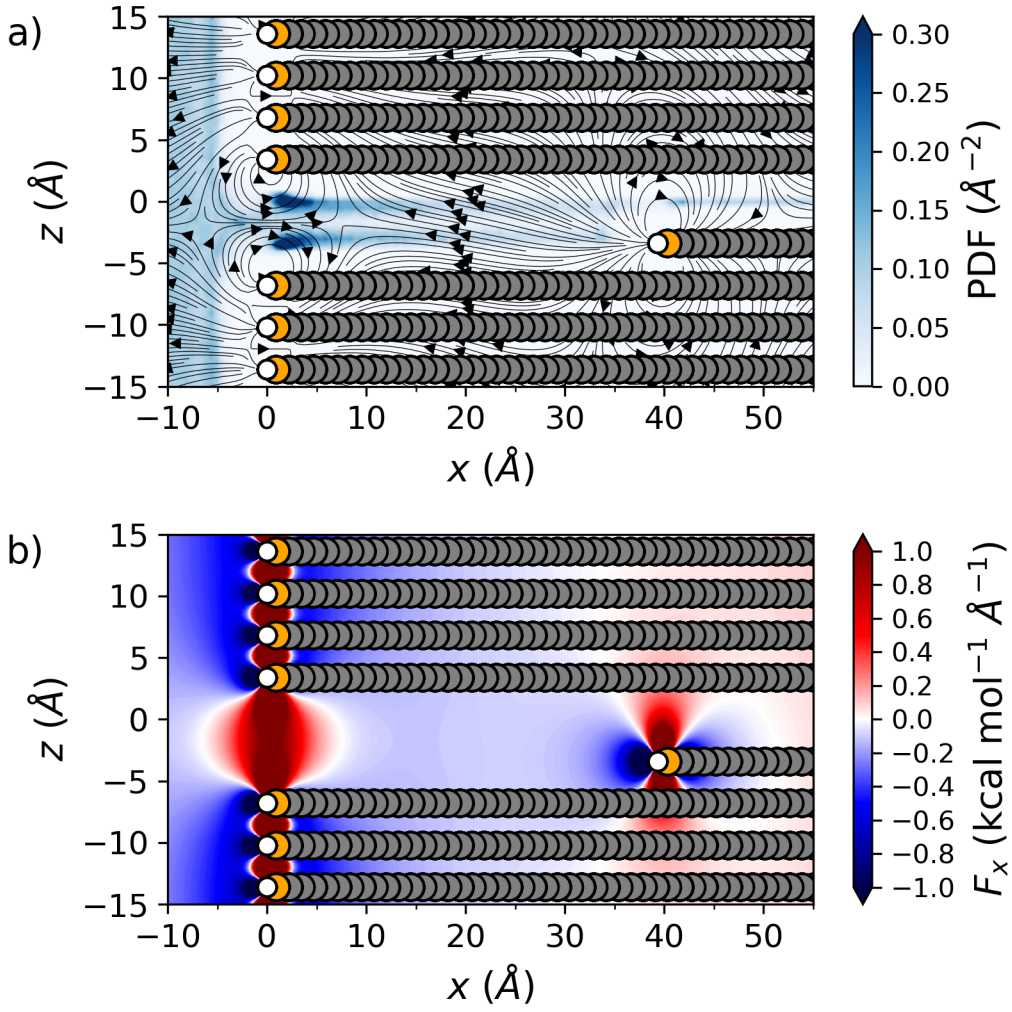

Figure S22: Probability Density and Electric Field Analysis for the ASC1 case. a) 2D Probability Density Function (PDFs). b) x-direction component of the net force (F_x) exerted by the functional group-generated electric field.

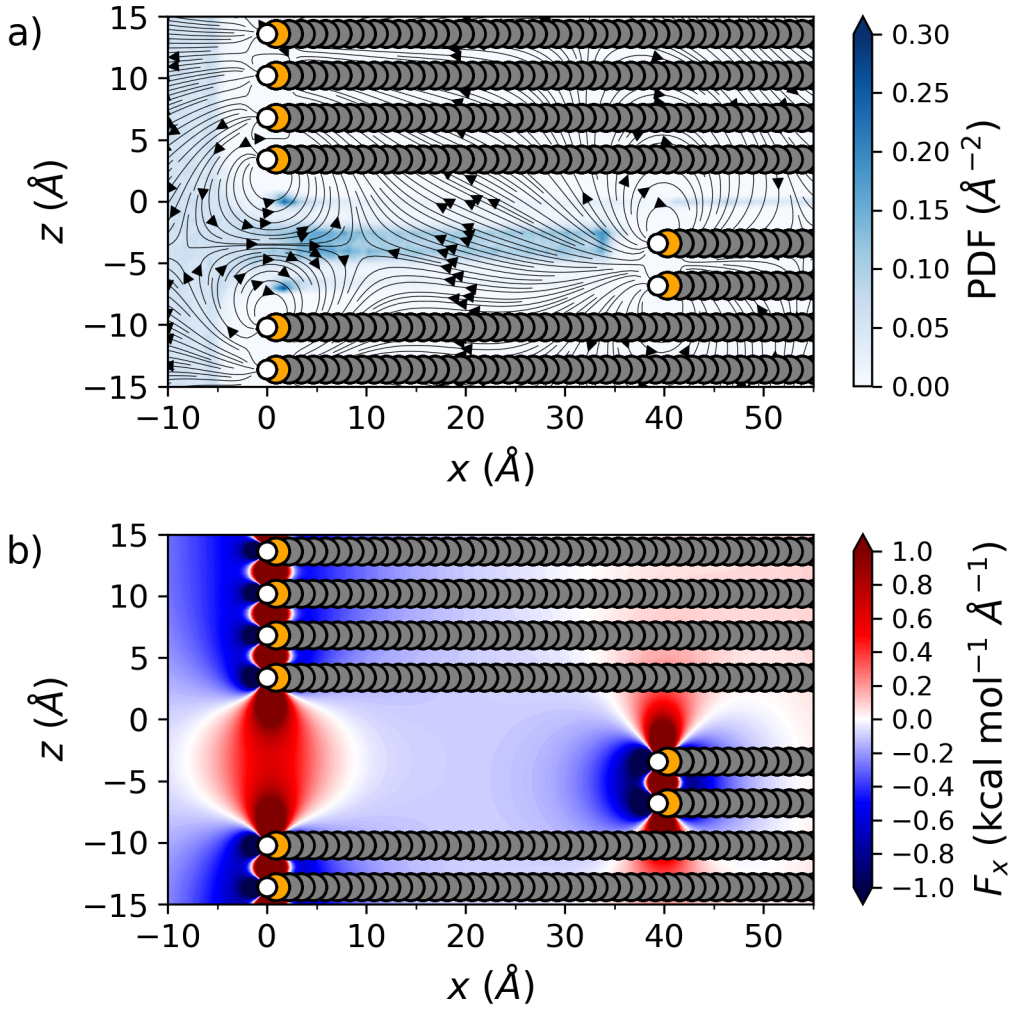

Figure S23: Probability Density and Electric Field Analysis for the ASC2 case. a) 2D Probability Density Function (PDFs). b) x-direction component of the net force (F_x) exerted by the functional group-generated electric field.

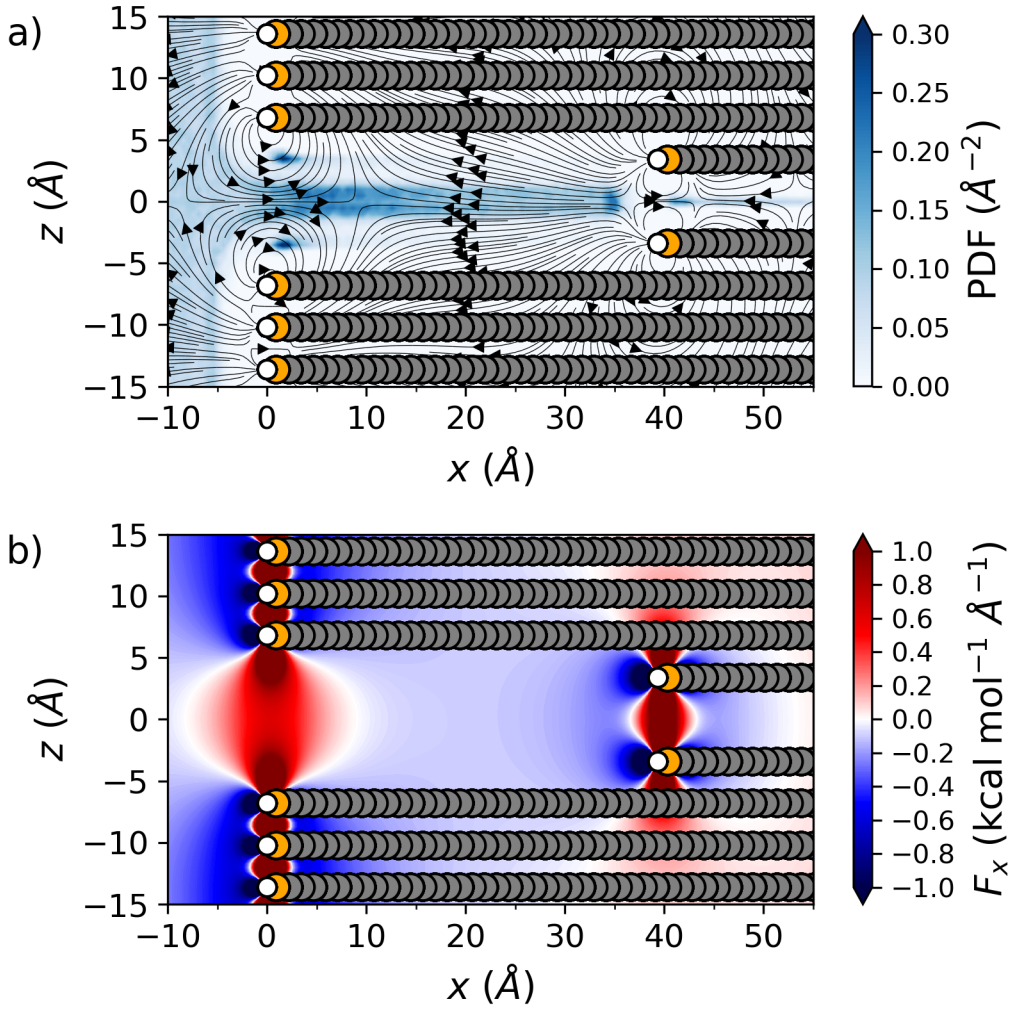

Figure S24: Probability Density and Electric Field Analysis for the SSC1 case. a) 2D Probability Density Function (PDFs). b) x-direction component of the net force (F_x) exerted by the functional group-generated electric field.

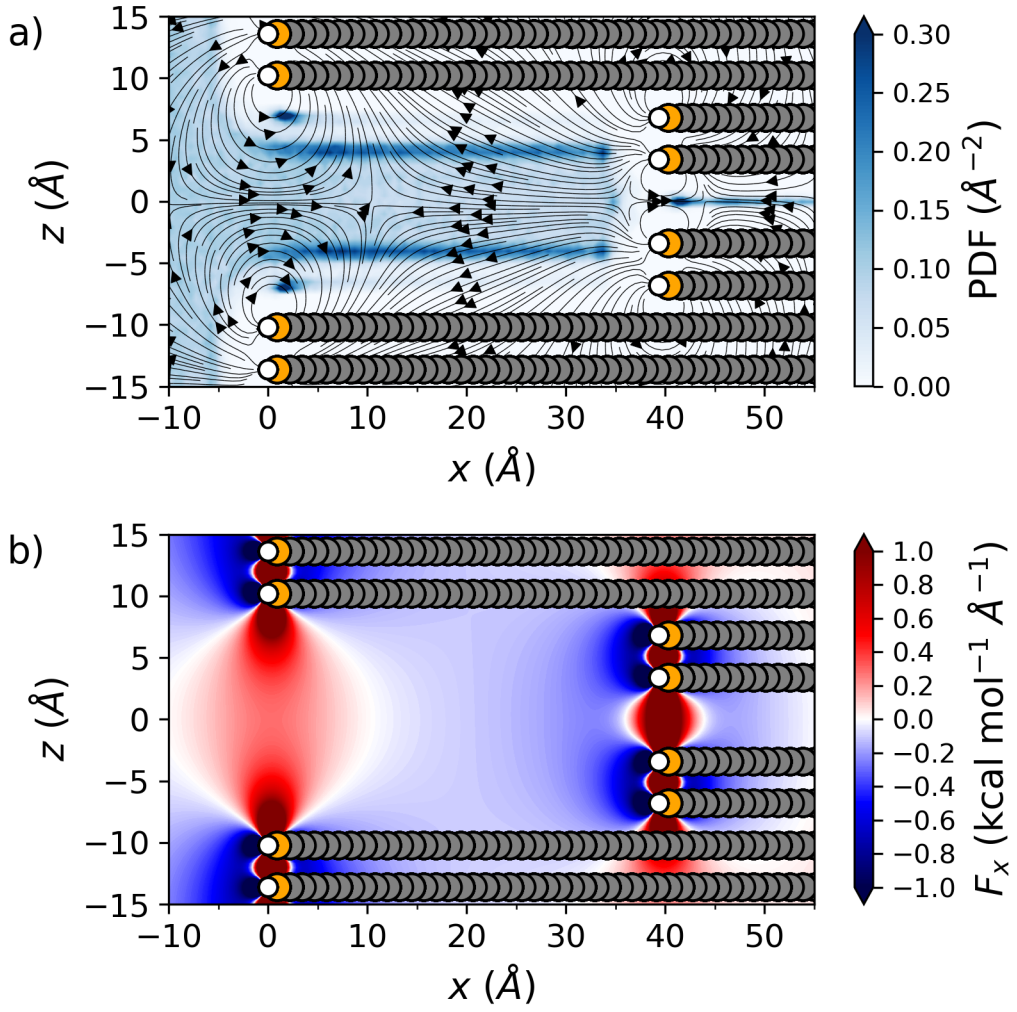

ž

Figure S25: Probability Density and Electric Field Analysis for the SSC2 case. a) 2D Probability Density Function (PDFs). b) x-direction component of the net force (F_x) exerted by the functional group-generated electric field.

10 Simulations of Na^+ conductance

To further probe the transport of cations across our membranes, we conducted an additional series of simulations, substituting the CsCl solution with a 1 M NaCl solution. In this section, we present the methodologies and results for this supplementary set of simulations.

10.1 Simulation overview (NaCl cases)

The simulation protocols are equal to those employed in the main set of simulations (transport of Cs^+). The membrane geometries evaluated here have the same characteristics as those for Cs^+. Each simulation employs an equal number of water molecules (see section 3 of the supporting information) than its correspondent Cs^+ case. Each system contains 32 Na^+ and 32 Cl^- ions per reservoir (which mirrors the 32 Cs^+ and 32 Cl^- for the main set of simulations). Each system is preequilibrated in the NPT ensemble (see section 10.2 of the supporting information). The transport of Na^+ is simulated in the NVT ensemble by applying electric fields ranging between 0.001 and 0.005 V/Å in the x direction. The applied electric fields correspond to applied voltages across the simulation box, ranging between 0.14 and 0.74 V.

10.2 Length of the simulation box in the x-direction (NaCl cases)

The employed length of the simulation box for each simulated case is presented in Table S5. The reported length is obtained after 4 ns of equilibration in the NPT ensemble (see 3). Similarly to the main set of simulations, the simulation box has lengths of 3.4 nm and 4.8 nm in $y-$ and $z-$directions, respectively.

10.3 Ionic current - Voltage (I-V) curves (NaCl cases)

The Ionic current - Voltage ($I-V$) curves for a 1M NaCl solution are presented for the Sharp, AA, SA, ASC, and SSC membrane geometries are presented in figs. S26, S27, S28,

Table S5: Length of the simulation box in the $x-$direction for each of the NaCl cases.

System	L_x (Å)
Sharp	152.76
AA1	145.95
AA2	146.84
AA3	145.95
AS1	145.26
AS2	145.86
AS3	145.55
ASC1	146.31
ASC2	146.25
SSC1	146.39
SSC2	146.13

S29, and S30, respectively. In all of the presented plots, error bars are estimated from the standard error of the computed ionic current.

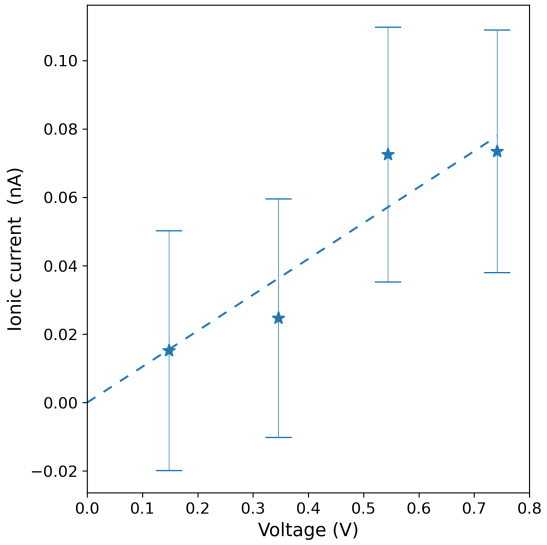

Figure S26: Ionic current - voltage ($I-V$) curves for a 1M NaCl solution in the Sharp geometry case.

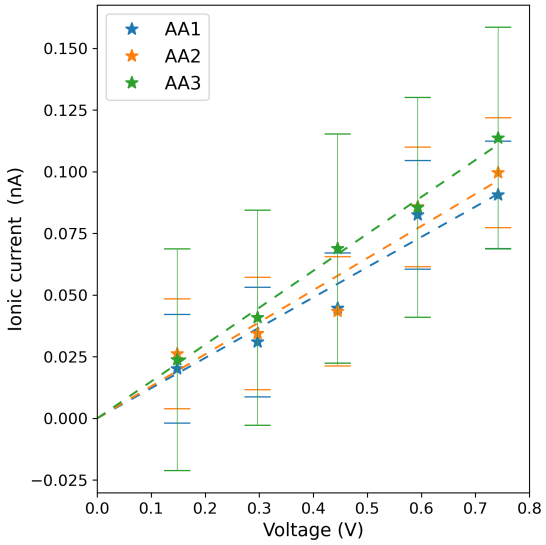

Figure S27: Ionic current - voltage ($I-V$) curves for a 1M NaCl solution in the AA geometry cases.

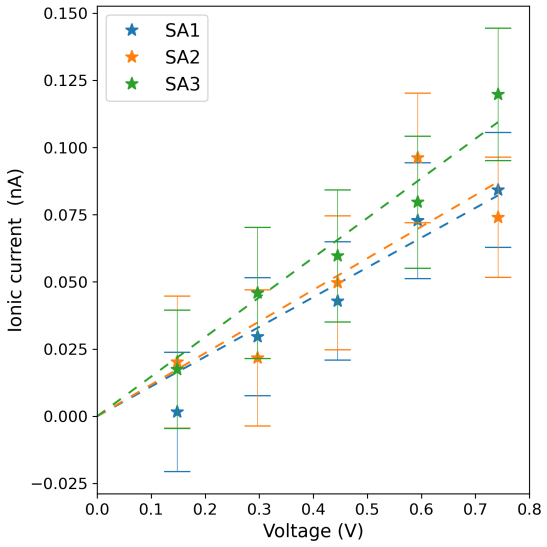

Figure S28: Ionic current - voltage ($I-V$) curves for a 1M NaCl solution in the SA geometry cases.

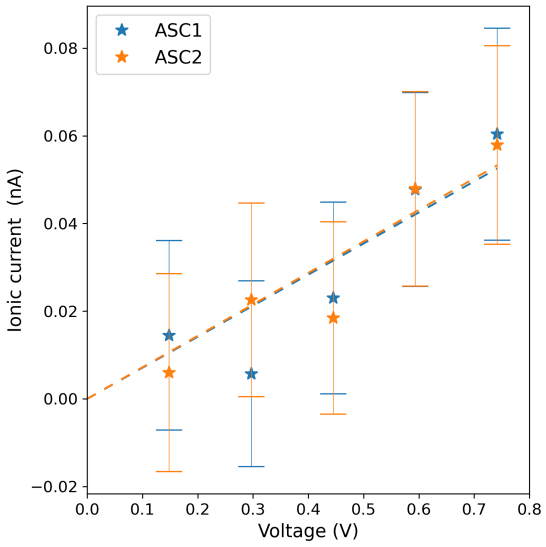

Figure S29: Ionic current - voltage ($I-V$) curves for a 1M NaCl solution in the ASC geometry cases.

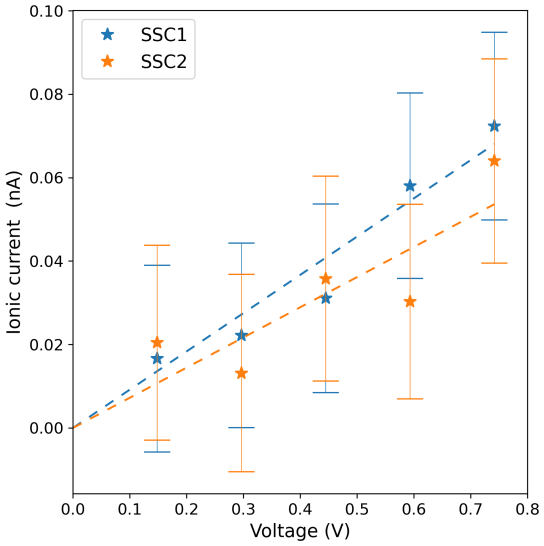

Figure S30: Ionic current - voltage ($I-V$) curves for a 1M NaCl solution in the SSC geometry cases. cases.

10.4 Hydration shell structure (NaCl cases)

The RDF for the Na^+-O and $Na^+ - H$ pairs in the thinner part of the membrane is presented in figure fig. S31. The RDFs for Na^+ in bulk solution is presented in figure fig. S32.

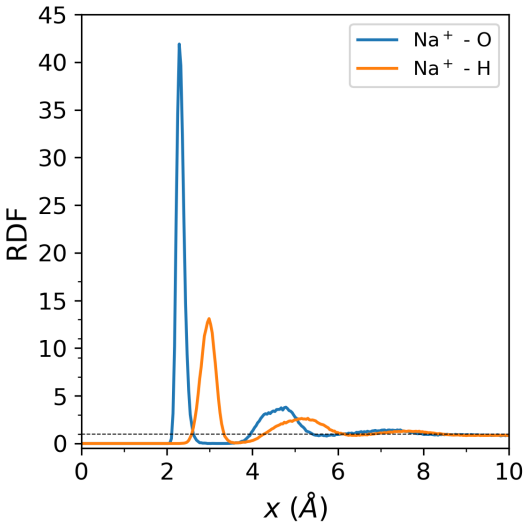

Figure S31: Radial density function for the Na^+-O and Na^+-H pairs for an ion confined in the $h_{eff} = 3.4$ Å channel

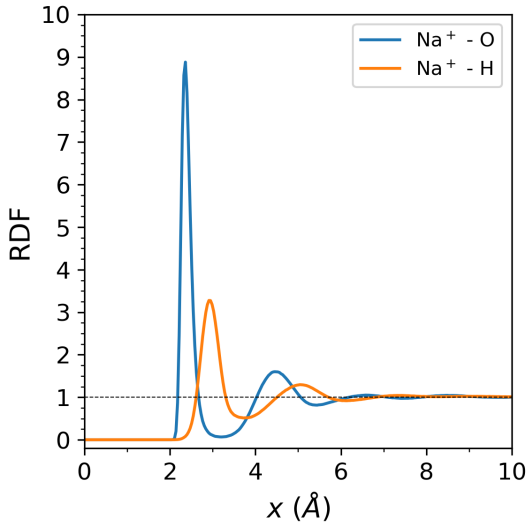

Figure S32: Radial density function for the Na^+-O and Na^+-H pairs for an ion in bulk aqueous solution

In bulk solution, i.e., outside the membrane, an average CN of 5.95 ± 0.1 was computed for the first hydration layer. Such a value is in close agreement with the values reported by Döpke et al.[S4]. The number of oxygen atoms in the second hydration layer for a Na^+ in bulk solution was determined to be 16.7 ± 0.8. When entering the thinner part of each membrane (with $h_{eff} = 3.4$ Å), the number of oxygen atoms in the first hydration layer is reduced to an average of 4.0 ± 0.1 atoms, while it is reduced to 7.6 ± 0.2 atoms in the second hydration layer. The distance between Na^+ and Oxygen atoms is reduced from ca. 2.37 Å in bulk solution to 2.29 Å in 2D confinement.

10.5 Potential of mean force (NaCl cases)

The estimated PMFs for the transport of Na^+ across the simulated membranes are presented in Figs. S33, S34, S35, and S36 for the AA, SA, ASC and SSC membrane geometries, respectively. In all these figures, the PMF for the transport of Na^+ in the Sharp membrane geometry is presented for comparison purposes.

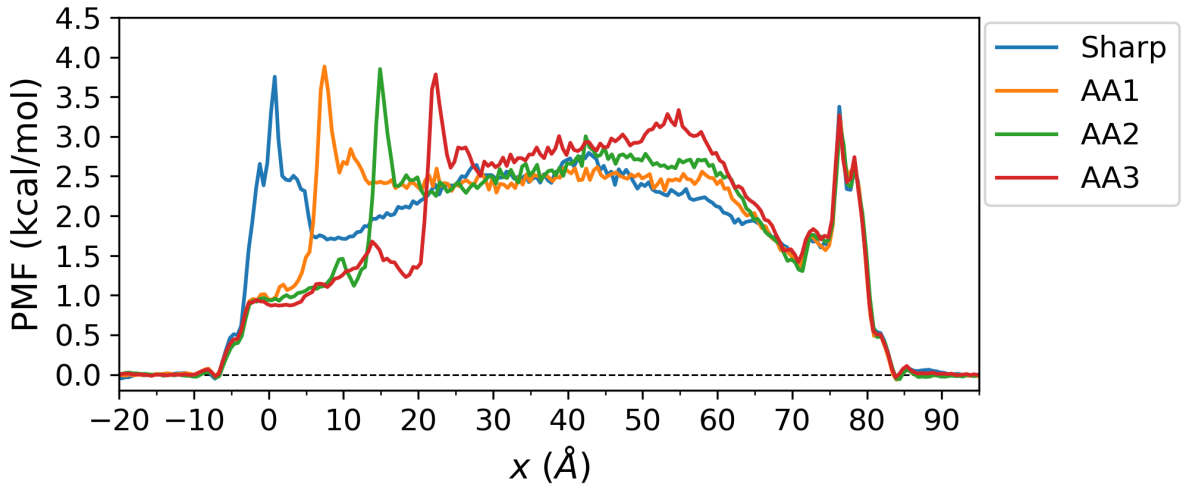

Figure S33: Potential of Mean Force (PMF) for the transport of Na^+ in the the AA membrane geometries.

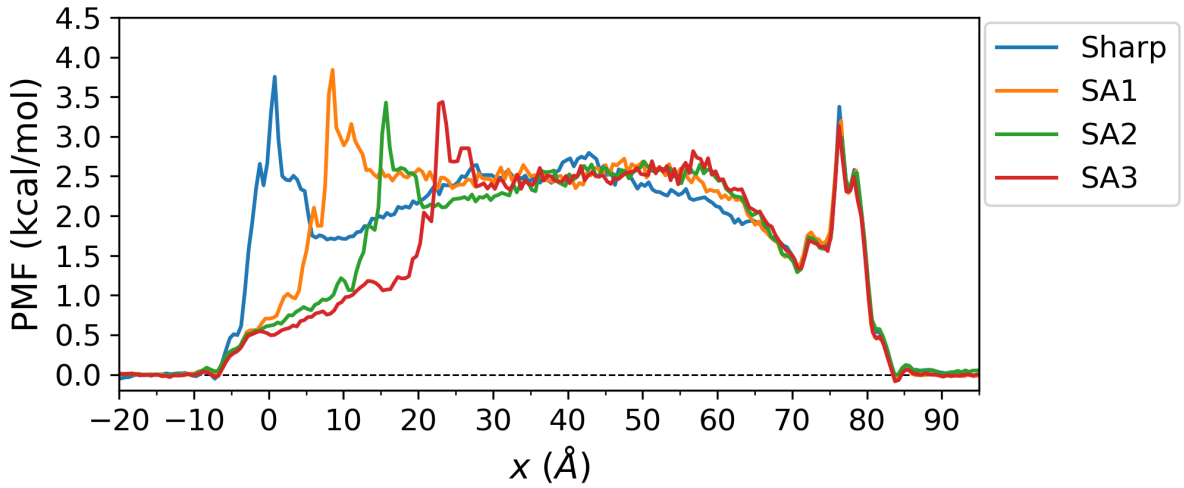

Figure S34: Potential of Mean Force (PMF) for the transport of Na^+ in the the SA membrane geometries.

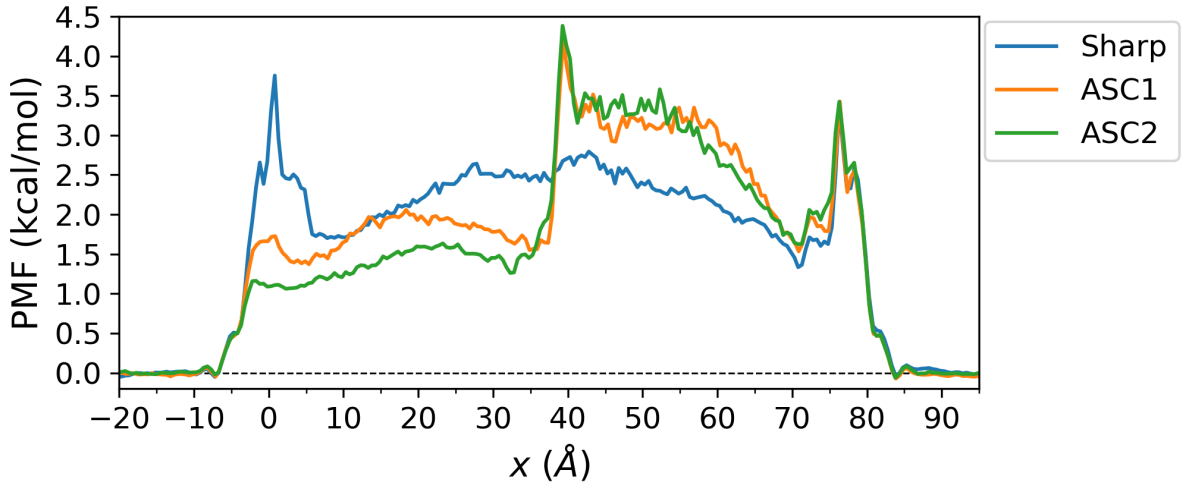

Figure S35: Potential of Mean Force (PMF) for the transport of Na^+ in the the ASC membrane geometries.

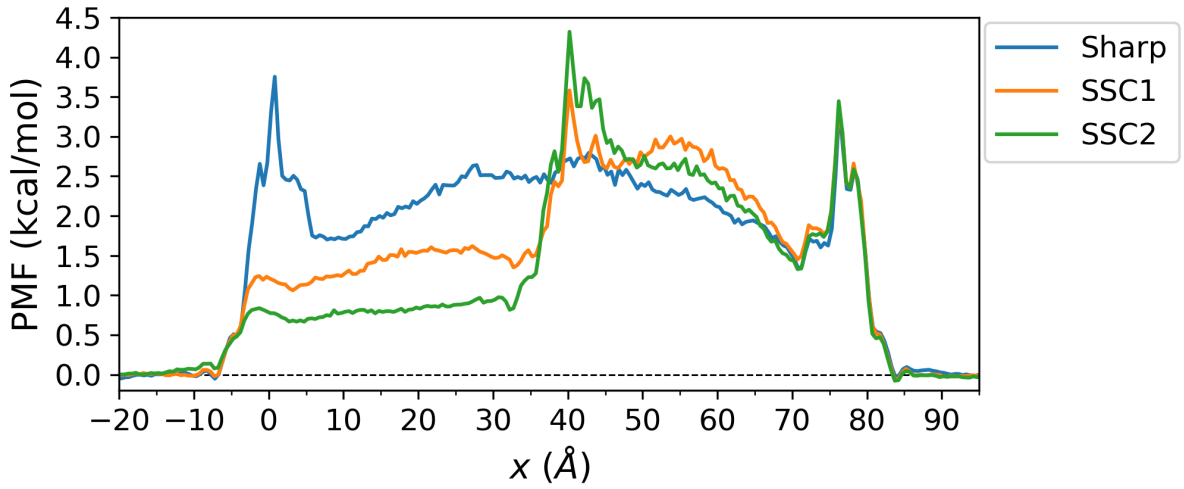

Figure S36: Potential of Mean Force (PMF) for the transport of Na^+ in the the SSC membrane geometries.

10.6 2D probability function (NaCl cases)

In this section, we present the 2D PDF for the NaCl cases. Notice that the $x-$component of the force exterted by electric field generated by the CH functional group is equal for the CsCl cases, thus is not presented here.

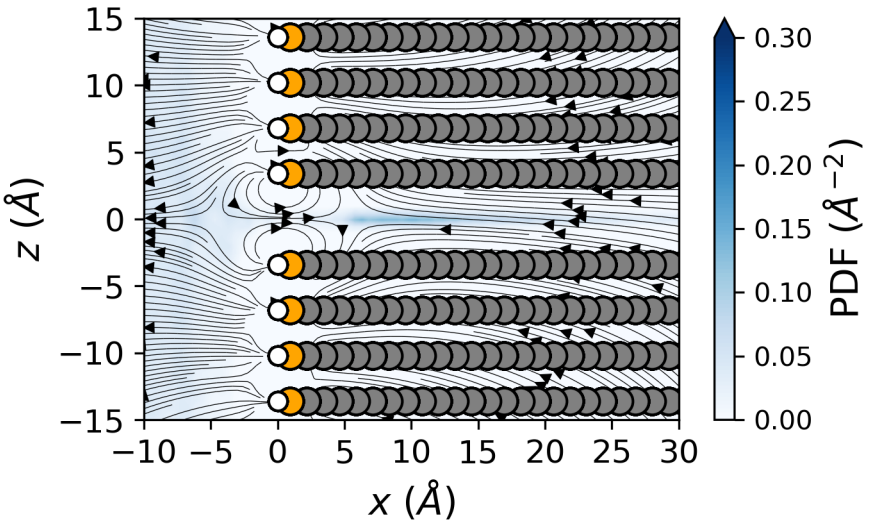

Figure S37: 2D Probability Density and Electric Field Analysis for a 1M NaCl solution in the Sharp geometry case.

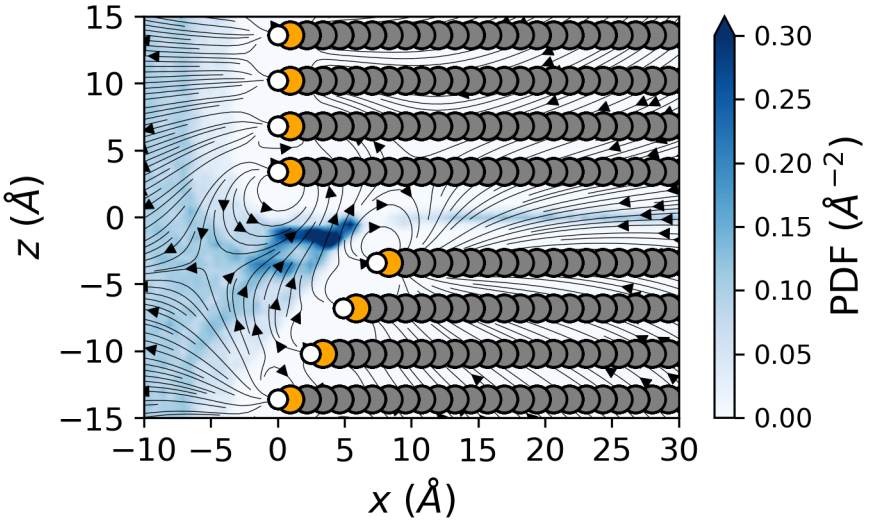

Figure S38: 2D Probability Density and Electric Field Analysis for a 1M NaCl solution in the AA1 geometry case.

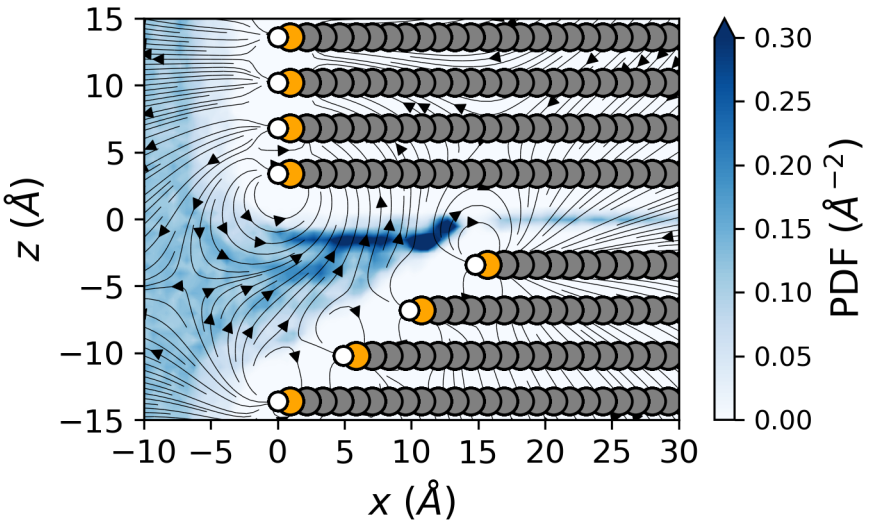

Figure S39: 2D Probability Density and Electric Field Analysis for a 1M NaCl solution in the AA2 geometry case.

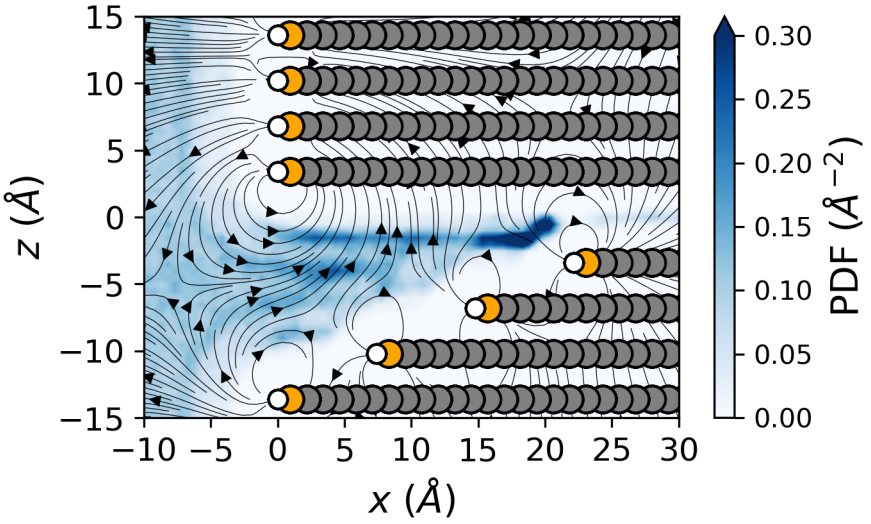

Figure S40: 2D Probability Density and Electric Field Analysis for a 1M NaCl solution in the AA3 geometry case.

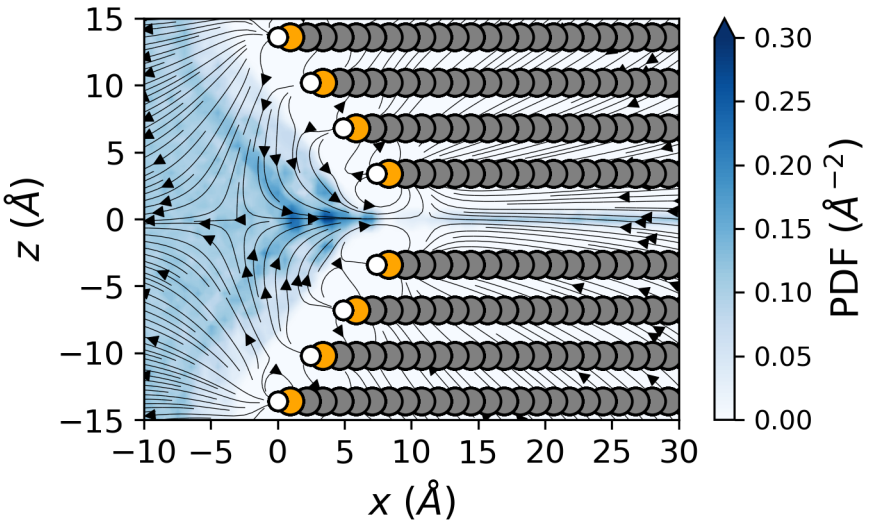

Figure S41: 2D Probability Density and Electric Field Analysis for a 1M NaCl solution in the SA1 geometry case.

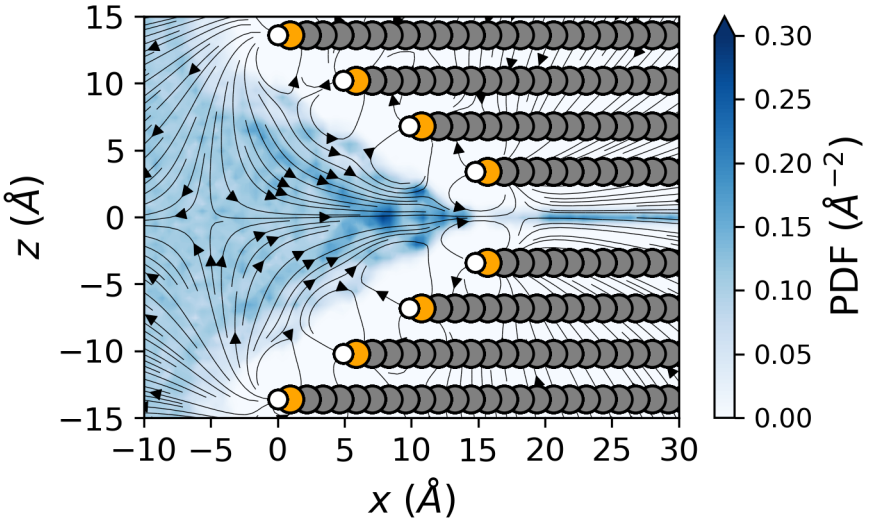

Figure S42: 2D Probability Density and Electric Field Analysis for a 1M NaCl solution in the SA2 geometry case.

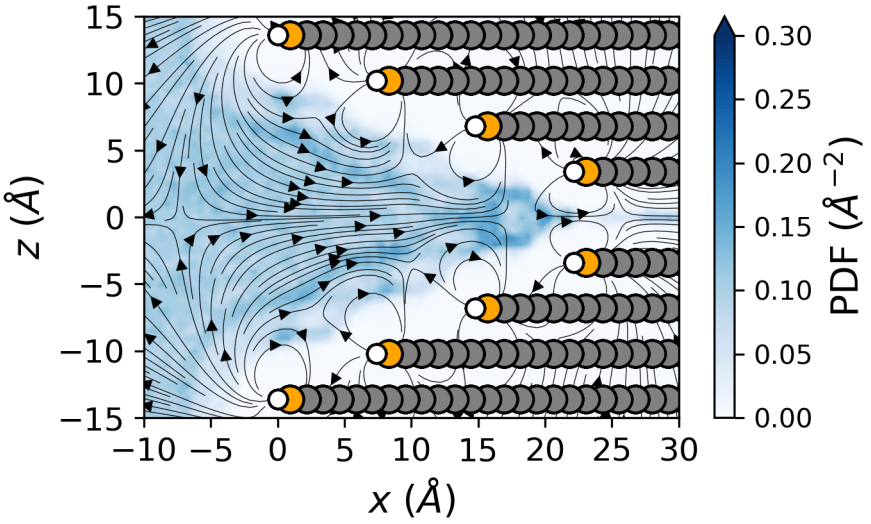

Figure S43: 2D Probability Density and Electric Field Analysis for a 1M NaCl solution in the SA3 geometry case.

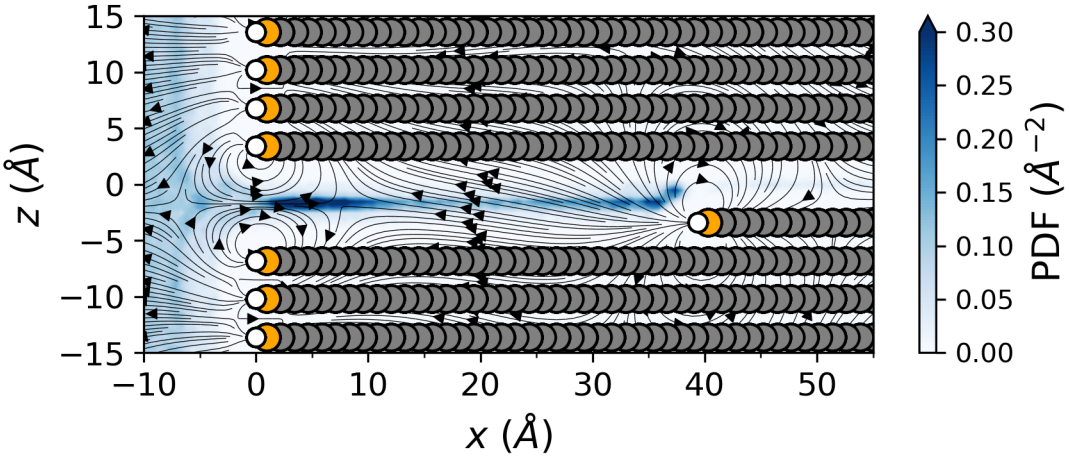

Figure S44: 2D Probability Density and Electric Field Analysis for a 1M NaCl solution in the ASC1 geometry case.

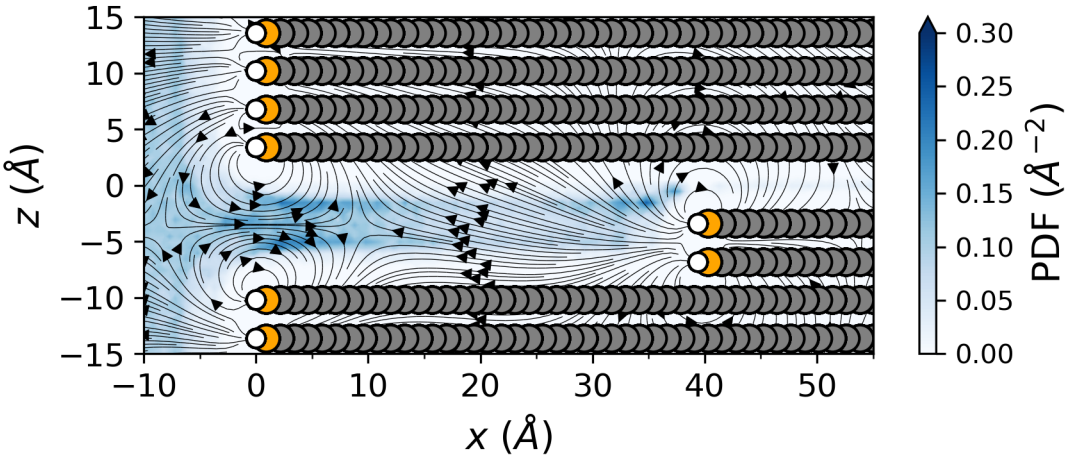

Figure S45: 2D Probability Density and Electric Field Analysis for a 1M NaCl solution in the ASC2 geometry case.

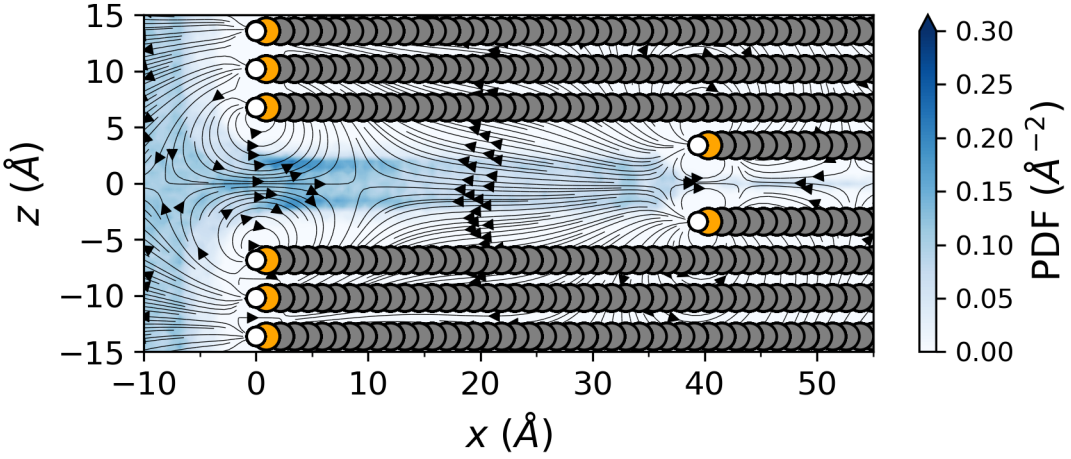

Figure S46: 2D Probability Density and Electric Field Analysis for a 1M NaCl solution in the SSC1 geometry case.

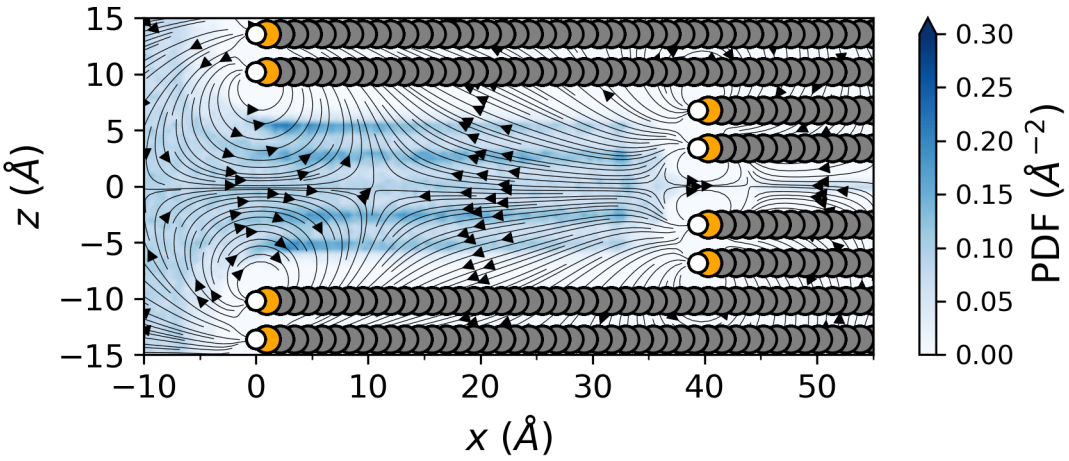

Figure S47: 2D Probability Density and Electric Field Analysis for a 1M NaCl solution in the SSC2 geometry case.

References

(S1) Abascal, J. L.; Vega, C. A general purpose model for the condensed phases of water: TIP4P/2005. *J. Chem. Phys.* **2005**, *123*, 234505.

(S2) Wang, J.; Cieplak, P.; Kollman, P. A. How well does a restrained electrostatic potential (RESP) model perform in calculating conformational energies of organic and biological molecules? *J. Comput. Chem.* **2000**, *21*, 1049–1074.

(S3) Joung, I. S.; Cheatham III, T. E. Determination of alkali and halide monovalent ion parameters for use in explicitly solvated biomolecular simulations. *The journal of physical chemistry B* **2008**, *112*, 9020–9041.

(S4) Döpke, M. F.; Moultos, O. A.; Hartkamp, R. On the transferability of ion parameters to the TIP4P/2005 water model using molecular dynamics simulations. *J. Chem. Phys.* **2020**, *152*, 024501.